

# The Ultraviolet Radiation Environment of a Tropical Megacity in Transition: Mexico City

## 2000-2019

Adriana Ipiña,<sup>\*,†,‡</sup> Gamaliel López-Padilla,<sup>¶</sup> Armando Retama,<sup>§</sup> Rubén D. Piacentini,<sup>†</sup> and Sasha Madronich<sup>||</sup>

<sup>†</sup>*Instituto de Física Rosario (CONICET-UNR), Rosario, Argentina*

<sup>‡</sup>*Centro de Ciencias de la Atmósfera, Universidad Nacional Autónoma de México, Mexico City, Mexico*

<sup>¶</sup>*Facultad de Ciencias Físico Matemáticas, Universidad Autónoma de Nuevo León, San Nicolás de los Garza, México*

<sup>§</sup>*Independent researcher, Mexico City, Mexico*

<sup>||</sup>*National Center for Atmospheric Research, Boulder, Colorado, USA*

E-mail: [ipina@ifir-conicet.gov.ar](mailto:ipina@ifir-conicet.gov.ar)

### Abstract

Tropical regions experience naturally high levels of UV radiation, but urban pollution can reduce these levels substantially. We analyzed 20 years of measurements of the UV Index (UVI) at several ground-level locations in the Mexico City Metropolitan Area and compared these data with UVI values derived from satellite observations of ozone and clouds (but not local pollution). The ground-based measurements were systematically lower than the satellite-based estimates, by ca. 40% in 2000 and 20% in 2019. Calculations with a radiative transfer model and observed concentrations of

9 air pollutants explained well the difference between satellite- and ground-based UVI,  
10 and showed specific contributions from aerosols in the boundary layer and the free tro-  
11 posphere, O<sub>3</sub>, NO<sub>2</sub>, and SO<sub>2</sub>, in decreasing order of importance. Such large changes  
12 in UV radiation between 2000 and 2019 have important implications ranging from hu-  
13 man health (skin cancer and cataract induction) to air pollution control (photochemical  
14 smog formation).

## 15 Introduction

16 Ultraviolet (UV) radiation is an important component of the urban environment, affecting  
17 human populations directly through UV exposure of skin and eyes<sup>1–3</sup> and less directly (but  
18 with great impact) by driving the formation of photochemical smog, including tropospheric  
19 ozone and other oxidants, as well as secondary aerosols containing nitrates, sulfates, and  
20 organics.<sup>4–6</sup> These pollutants, along with others of primary origin commonly found in ur-  
21 ban atmospheres (e.g., black carbon, sulfur dioxide), can in turn scatter and/or absorb UV  
22 radiation, alter its vertical distribution, and so modify the photochemical rate of their own  
23 formation. Such feedback complicates the calculation of both the UV radiation field (in-  
24 cluding at the surface), and the evolution of photochemical smog in the urban boundary  
25 layer.

26 The question of how air pollution alters the urban UV environment (and *vice versa*) is  
27 not new, but studies have relied mostly on numerical models,<sup>7–9</sup> with relatively few available  
28 observations (e.g., McKenzie et al.<sup>10</sup>, Panicker et al.<sup>11</sup>, Palancar et al.<sup>12</sup>, reviewed by Bais  
29 et al.<sup>13</sup>). Increases in UV have been estimated as a consequence of emission reductions  
30 over the last decades, e.g. in China,<sup>14–16</sup> and have led to less-than-expected reductions in  
31 photochemical smog, in part due to stronger UV photochemistry.<sup>17? ,18</sup> Emission reductions  
32 have also occurred globally during the 2020 COVID-19 pandemic,<sup>19,20</sup> but ground-level ozone  
33 in some polluted areas has actually increased,<sup>21,22</sup> due at least in part to the increased UV  
34 radiation. Unfortunately, the observational data base of relevant UV radiation remains

35 rather sparse to evaluate such model-derived hypotheses.

36 The environment of Mexico City is of particular interest for several reasons: (1) Nearly  
37 23 million people inhabit the Mexico City Metropolitan Area (MCMA), and the UV en-  
38 vironment has direct implications for their health, both in terms of skin/eye UV exposure  
39 and *via* photochemical smog formation. (2) As a tropical megacity, it is to some extent  
40 representative of the situation of many others, with year-round intense midday UV irradia-  
41 nce, a shallower atmosphere due to the city's high elevation of 2240 m above sea level,  
42 and a transition toward newer and cleaner technologies, leading to gradual improvements  
43 in air quality. (3) Air quality within MCMA has undergone extensive scrutiny, with a well-  
44 established monitoring network operating since 1986,<sup>23</sup> numerous intensive field campaigns  
45 to study the meteorology, emissions, and photochemistry of smog formation,<sup>24–26</sup> and numer-  
46 ical modeling incorporating the evolving knowledge.<sup>27–30</sup> This extensive body of knowledge  
47 provides the foundation for understanding our study.

48 Here, we analyze two decades of continuous measurements of the UV Index at multiple  
49 locations within the MCMA, collected by the Secretariat of the Environment (Secretaría  
50 del Medio Ambiente, SEDEMA)<sup>1</sup> of the Mexico City government as part of an intensive  
51 monitoring network over the MCMA. The UV Index is defined as:

$$UVI = 40 \int_{250nm}^{400nm} E(\lambda, t) \cdot S_{er}(\lambda) d\lambda \quad (1)$$

52 where  $E(\lambda, t)$  is the solar spectral irradiance in units of  $\text{W} \cdot \text{m}^{-2} \cdot \text{nm}^{-1}$  and  $S_{er}(\lambda)$  is  
53 the erythemal sensitivity of human skin.<sup>31,32</sup> Multiplication by 40 was chosen historically to  
54 express the UVI in small integer numbers, but is otherwise scientifically arbitrary.

55 The UVI is recognized by the World Health and Meteorological Organizations (WHO  
56 and WMO) as a standardized metric of UV radiation<sup>31</sup> for global public information. An  
57 advantage of using the UVI as (one) measure of UV radiation is that it is being increasingly  
58 observed or calculated and disseminated, enabling more objective comparisons among seasons

---

<sup>1</sup><https://www.sedema.cdmx.gob.mx/>

59 and locations. The UVI observations from Mexico City, considered here, are an important  
60 element of this global picture.

61 While the UVI at the surface cannot be translated directly into photolysis frequencies  
62 for various photo-labile molecules, the spectral weighting of the UVI (ca. 300-320 nm) is  
63 approximately similar to that for the photolysis of ozone to singlet oxygen atoms. Other UV  
64 wavelengths are of course also important, e.g. for the photolysis of nitrogen dioxide, and  
65 may be affected differently depending on the pollutant. With these considerations and a few  
66 other caveats, UVI trends examined here can also be used to infer accompanying trends in  
67 photolysis frequencies and influences on photochemical smog formation.

## 68 Methods

### 69 Ground-based measurements

70 The Mexico City Metropolitan Area is located at 19.4°N, 99.1°W, 2240 meters above sea  
71 level (m asl), surrounded by mountain ridges exceeding 5000 m asl, with complex topog-  
72 raphy and thermal inversions that inhibit winds and favor intense air pollution.<sup>33-35</sup> Air  
73 quality monitoring and surface meteorological measurements in the MCMA are conducted  
74 continuously by the Automated Atmospheric Monitoring Network (RAMA, by its Spanish  
75 acronym) of the Atmospheric Monitoring System (SIMAT, by its Spanish acronym) of the  
76 Mexico City government. Since the year 2000, UV radiometers (model 501-A, Solar Light  
77 Company Inc., Glenside, PA) detecting wavelengths between 280-400 nm have been mea-  
78 suring erythemally-weighted solar radiation. The calibration of the UV sensors has been  
79 carried out annually by comparing against a factory-calibrated reference sensor. The out-  
80 put voltages from the network's sensors have been compared for at least one week against  
81 the UV readings from the reference sensor to derive a calibration factor. New calibration  
82 factors typically differ from the old ones by 2% or less. Reference sensors have been also  
83 calibrated by the manufacturer and updated periodically (between 3 to 5 years) to reduce

84 systematic errors due to drifts in sensitivity. Long term calibration drift are minimized by  
 85 these yearly re-calibrations. Although at the beginning only a few stations were in oper-  
 86 ation and have been changing, currently 11 stations are recording erythemal irradiances,  
 87 which are then multiplied by 40 (see Eq. 1) to give UV Indices. Table 1 describes the lo-  
 88 cation of the stations where the UV Index has been measured. Figure 1 shows how the  
 89 radiometers of the SIMAT have been distributed over MCMA, prioritizing sites with higher  
 90 population density. Near real-time data for each station are available on the SIMAT official  
 91 website <http://www.aire.cdmx.gob.mx/default.php>. Daily maximum values ( $UVI_{max}$ )  
 92 were extracted in each of the stations around solar noon from the time interval from 11:00  
 93 h-15:00 h CST (Central Standard Time). This database with 7305 continuous days of mea-  
 94 surements during the period 2000-2019 was analyzed.

Table 1: SIMAT stations and AERONET site\*, environmental descriptors and geographical positions. Abbreviations names: Chalco (CHA), Cuautitlán (CUT), FES Acatlán (FAC), Hangares (HAN), Laboratorio de Análisis Ambiental (LAA), Merced (MER), Montecillo (MON), Milpa Alta (MPA), Pedregal (PED), San Agustín (SAG), Santa Fe (SFE), Tlalnepantla (TLA) and National Autonomous University of Mexico (UNAM\*)

Station	Environment	Lat (°N)	Lon (°W)	El (m asl)
CHO	semi-urban	19.27	98.89	2253
CUT	ecological park	19.72	99.20	2263
FAC	urban	19.48	99.24	2299
HAN	urban	19.42	99.08	2235
LAA	urban	19.48	99.15	2255
MER	downtown	19.42	99.12	2245
MON	rural	19.46	98.90	2252
MPA	rural	19.18	98.99	2594
PED	residential	19.33	99.20	2326
SAG	urban	19.53	99.03	2241
SFE	residential	19.36	99.26	2599
TLA	urban	19.53	99.20	2311
UNAM*	University city	19.33	99.18	2294

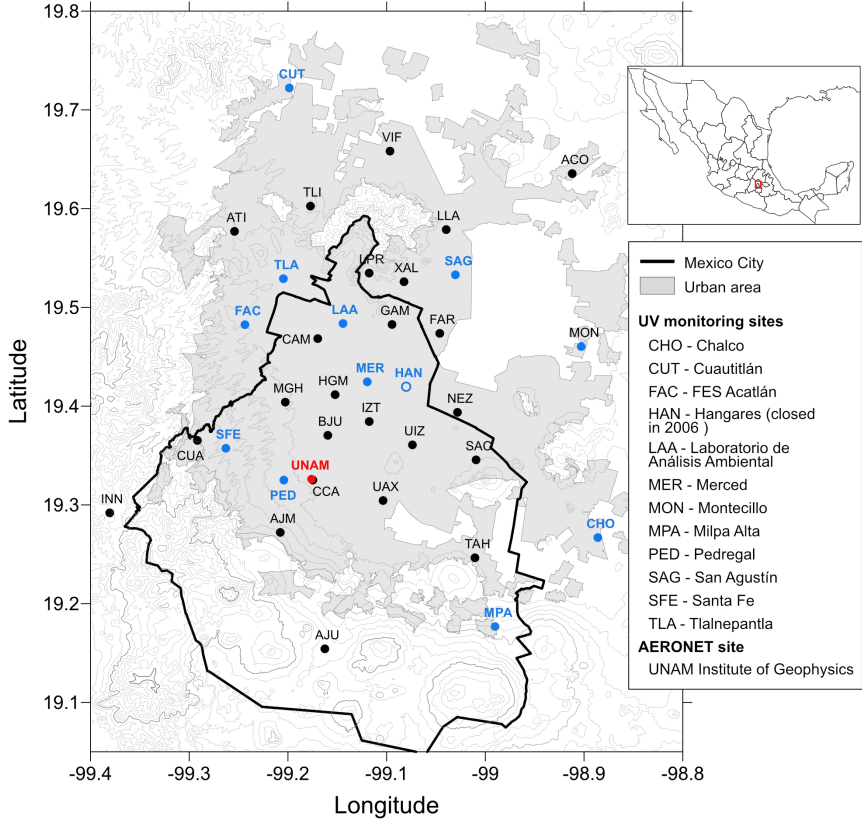


Figure 1: Map with the location of the SIMAT continuous monitoring stations over MCMA. Sites denoted by the blue solid dots correspond to SIMAT stations with UV measurements, while the black dots indicate SIMAT stations without UV measurements, the site indicated by an open blue dot represents a discontinued site, the red dot shows the location of the AERONET site. The location of Mexico City and the acronyms of the UV and AERONET site are shown at the upper and lower frames at the right respectively.

With the aim to explore the relationship between UVI and air pollutants levels, the hourly averages for ozone ( $O_3$ ), carbon monoxide (CO), nitrogen dioxide ( $NO_2$ ), sulfur dioxide ( $SO_2$ ) and particle matter with diameter sizes  $\leq 10 \mu m$  ( $PM_{10}$ ), were downloaded from the SIMAT.<sup>?</sup> For purposes of assessing the influence on the UV Index at solar noon, only values obtained between 11h and 15h CST were considered for the trends analysis. Pollutant measurements are conducted by the SIMAT using regulatory-grade commercial instruments. Measurement principles include ultraviolet photometry (model 400E, Teledyne-API) for  $O_3$ , chemiluminescence (model 200E, Teledyne-API) for  $NO_2$ , UV fluorescence (model 100E, Teledyne API) for  $SO_2$ , and infrared absorption (model 300E, Teledyne-API) for CO.

<sup>104</sup> The PM<sub>10</sub> continuous mass concentration was measured with Tapered Element Oscillating  
<sup>105</sup> Microbalance (TEOM 1400AB or TEOM 1405 DF, Thermo Scientific) monitors. Gaseous  
<sup>106</sup> pollutant levels are reported in ppb concentration units for O<sub>3</sub>, SO<sub>2</sub> and NO<sub>2</sub>, and in ppm  
<sup>107</sup> for CO. Particulate matter mass concentration is reported in  $\mu\text{g m}^{-3}$  at local conditions for  
<sup>108</sup> temperature and pressure.

<sup>109</sup> Aerosol optical depth at 340 nm was obtained from the Institute of Geophysics of the  
<sup>110</sup> National Autonomous University of Mexico (UNAM). Measurements were conducted with  
<sup>111</sup> a CIMEL sun photometer model CE-318, which is an automatic sun-sky-scanning spectral  
<sup>112</sup> radiometer of the AErosol RObotic NETwork (AERONET<sup>36</sup>). The data Product Level 2.0  
<sup>113</sup> and 1.5 (only in 2019) were selected, and annual averages AOD<sub>340</sub> were calculated along  
<sup>114</sup> the period 2000-2019, except for the year 2011 due to there were no measurements. A  
<sup>115</sup> previous study of the AOD behavior from 2000 to 2014 demonstrated that data gaps did not  
<sup>116</sup> significantly change the trends calculated for this.<sup>37</sup> Only 8% of the data between the years  
<sup>117</sup> 2014 and 2019 were missing. The largest data gap occurred in 2018 when the instrument  
<sup>118</sup> was returned for calibration.

## <sup>119</sup> Satellite data

<sup>120</sup> The UV Index data derived from satellite measurements of reflected radiance were used for  
<sup>121</sup> comparison with the ground-based measurements. These data were provided by the Ozone  
<sup>122</sup> Monitoring Instrument (OMI) on board of AURA-NASA satellite.<sup>38</sup> OMI is operated in co-  
<sup>123</sup> operation between the Netherlands Agency for Aerospace Programmes (NIVR), the Finnish  
<sup>124</sup> Meteorological Institute (FMI) and NASA. OMI performs observations over a geographical  
<sup>125</sup> area of 13×24km<sup>2</sup> at nadir. For the coordinates (19.33°N, 99.18°W) and elevation (2268 m  
<sup>126</sup> asl) of Mexico City, the satellite overpass time is between 19:00h - 21:00h UTC (20:00h -  
<sup>127</sup> 22:00h CET). Measurements of the ozone profile and the attenuation by clouds are used  
<sup>128</sup> via a radiative transfer model to estimate the UVI at the ground.<sup>39</sup> The UV Index used for  
<sup>129</sup> Mexico City corresponds to values at local noon time and clear sky from OMUVB Level 2

<sup>130</sup> OVP data product, version 1.3 and collection 3.

## <sup>131</sup> TUV model

<sup>132</sup> Calculations of the UV Index were also made with the Tropospheric Ultraviolet Visible (TUV  
<sup>133</sup> v5.3) model.<sup>40</sup> The model atmosphere is represented by 80 vertical layers, each 1 km thick,  
<sup>134</sup> starting at the 2.24 km asl elevation of MCMA, and for which the first three km constitute  
<sup>135</sup> the atmospheric boundary layer (BL).<sup>41</sup> The ozone profile above the BL is from the US  
<sup>136</sup> Standard Atmosphere, but rescaled to a value of 259.6 DU. Total ozone columns including  
<sup>137</sup> the BL contributions (of 13.7 DU in the year 2000 and 9.8 DU in 2019, see below) were  
<sup>138</sup> 273.1 DU in 2000 and 269.2 DU in 2019, respectively. The climatological O<sub>3</sub> column for this  
<sup>139</sup> latitude and season is about 270 DU (plus or minus ca. 5 DU) so in good agreement with  
<sup>140</sup> the values used here.

<sup>141</sup> Pollutants within the BL (including O<sub>3</sub>) are assumed to be well mixed, in agreement with  
<sup>142</sup> observations from the MILAGRO field campaign that showed the disappearance of vertical  
<sup>143</sup> gradients in the profiles of gases<sup>42,43</sup> and aerosols<sup>44,45</sup> by late morning. The UV-absorbing  
<sup>144</sup> gases considered here are O<sub>3</sub>, NO<sub>2</sub>, and SO<sub>2</sub>, specified in ppb.

<sup>145</sup> BL aerosols are modeled by prescribing the AOD at 340 nm (from AERONET observa-  
<sup>146</sup> tions), scaled to other wavelengths inversely with wavelength (Angstrom coefficient = 1.0),  
<sup>147</sup> asymmetry factor of 0.7, and a single scattering albedo of 0.85 at UV wavelengths, following  
<sup>148</sup> the determinations made in Mexico City by Corr et al.<sup>46</sup> and Palancar et al.<sup>12</sup>.

<sup>149</sup> Above the atmospheric boundary layer, the model atmosphere was specified to be, NO<sub>2</sub>,  
<sup>150</sup> or SO<sub>2</sub>. In one sensitivity study, a total AOD of 0.7 was redistributed placing 0.2 in the free  
<sup>151</sup> troposphere (decreasing vertically with an exponential scale height of 4 km, and 0.5 remaining  
<sup>152</sup> in the BL). The calculated UVI differed by less than 1%. Thus, as long as the total AOD  
<sup>153</sup> is known, knowledge of the exact vertical aerosol profile is not critical for ground-level UVI  
<sup>154</sup> but would obviously affect the vertical structure of photolysis frequencies.

<sup>155</sup> Radiative transfer calculations were carried out with the pseudo-spherical 4-stream op-

156 tion, at 1 nm steps between 280 and 400 nm.

## 157 Results and Discussion

158 Figure 2 shows the diurnal variation of the UVI for several specific cloud-free days, for  
159 different seasons and several locations (CHO, MER, MON, PED, SAG, SFE and TLA).  
160 UV Index calculated with the TUV model was used as reference of the behavior during  
161 clear sky days. According to the comparison of measurements minute by minute, the dates  
162 with prolonged fluctuations along the day were discarded. However, during the rainy period  
163 (from June to October) at least a brief episode of clouds, as shown at CHO station around  
164 noon in 13 June 2017. Peak values range from 8 during autumn/winter to above 12 in  
165 spring/summer, in correspondence to the respective December and June solstices. Although  
166 the stations are all within a 25 km radius, substantial differences among them are notable.  
167 Survey of the locations revealed that shadowing from nearby structures is not an issue. The  
168 good agreement in the morning, followed by more divergence in the afternoon, is consistent  
169 with the development of photo-chemical pollution hotspots during the day. Previous studies  
170 (e.g., Castro et al.<sup>47</sup> and Palancar et al.<sup>12</sup>) have shown that surface UV radiation in Mexico  
171 City is attenuated significantly by aerosols. The measurements shown in Fig. 2 are consistent  
172 with this increasing pollution during the course of the day, with highest aerosol loading (and  
173 highest variability) attained in the afternoon. Further support for the role of pollution in  
174 suppressing the UVI comes from the observation made at the Santa Fe (SFE) site which in  
175 Fig. 2 are seen to be systematically higher, e.g. by over 10% in autumn afternoons, compared  
176 to the other stations. The SFE station is displaced to the west from the majority of the other  
177 stations, and remains in the outskirts. This site is also approximately 300 m higher than  
178 Mexico City downtown, so that the cleaner atmosphere at SFE is a result of the station's  
179 location farther away from pollution sources, both horizontally and vertically.<sup>48</sup> It is indeed  
180 expected to have higher values of the UVI, in agreement with the observations.

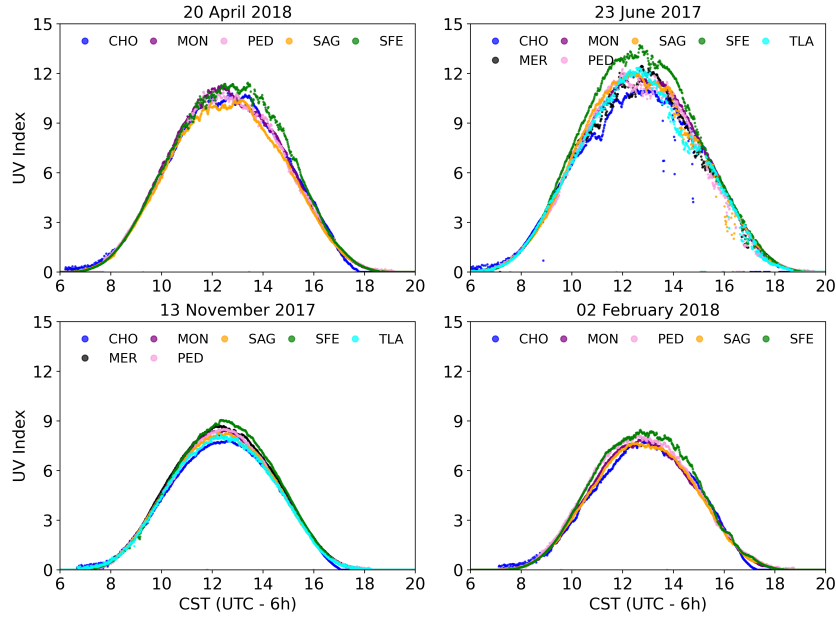


Figure 2: UV Index measurements at 1-minute resolution from several SIMAT stations within the MCMA under mostly cloudless conditions for representative days of the year.

181 The daily maximum UV Index of each station is denoted by  $UVI_{max}$ , these values were

182 counted in the period 2000-2019. As shown in Figure 3, these values ranged from 1 to

183 16, with a majority (61%) of the days experienced  $UVI_{max}$  values between 6 and 10, and

184 remarkably few, less than 1%, in the 13-16 range. The lowest values are likely due to winter

185 days with heavy cloud cover and low sun angles, and UV attenuation by pollutants could

186 also be amplified under such conditions, due to longer photon path lengths at low sun and

187 within clouds. The extreme sparsity of high UVI values remains surprising, and may be an

188 indication of the rarity of extremely unpolluted days within the city.

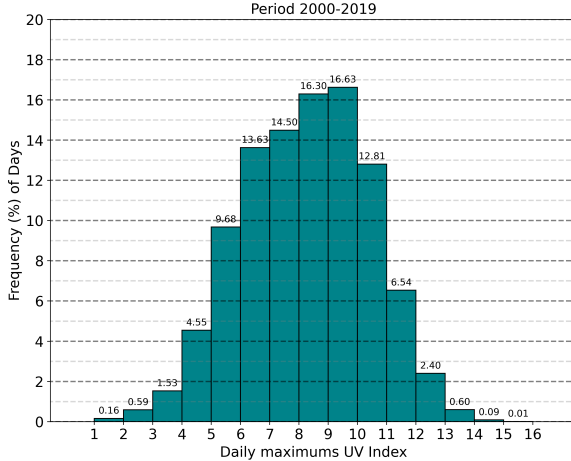


Figure 3: Frequency distribution of daily maximums UV Index values in Mexico City during 2000 -2019.

189 Similar patterns are found when considering the monthly average of the  $UVI_{\max}$  values

190 as shown in Figure 4. The long-term averages present a seasonal variation (as in Fig. 2) that

191 follows approximately the cosine of the noontime solar zenith angle. Notably, values rarely

192 if ever exceed 12 (as in Fig. 3). The lowest average UVI (near 7) occurs in winter while

193 from March to August the values seem to be flattened in the range 10-11. The rather low

194 monthly UV Index values could be a consequence of the presence of clouds in the rainy season.

195 However, urban aerosol pollution sources, biomass burning for agriculture and wood cooking

196 also contribute to poor air quality between March-May<sup>49</sup>. Using the maximum  $UVI_{\max}$  from

197 all of stations every day (one daily point), the monthly averages ( $\overline{UVI}_m$ ) were calculated

198 along the period 2000-2019 (except for June 2003 due to there were no measurements). Long

199 term trends in  $\overline{UVI}_m$  are shown in Figure 5. A clear upward trend is seen, with a slope for

200 the linear fit of 0.9%/year or +1.5 UVI units over the two decades.

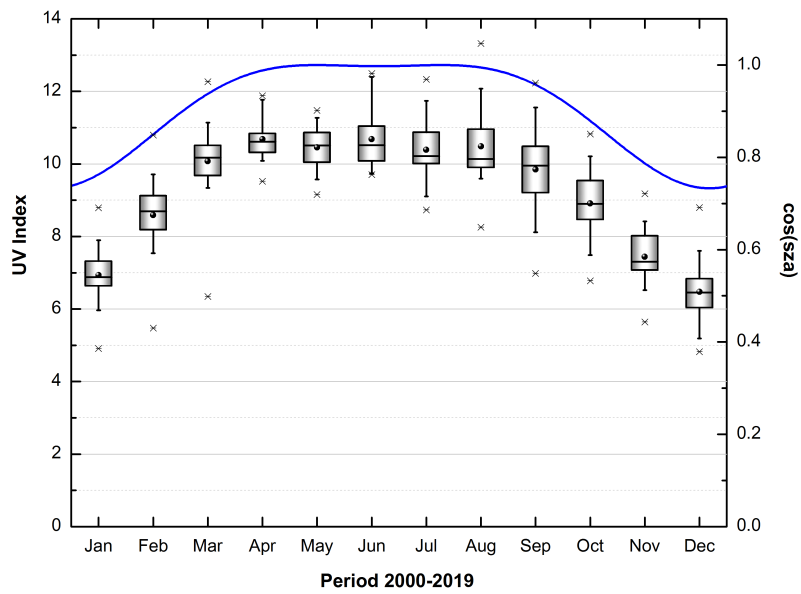


Figure 4: Boxplot of the monthly averages of the maximum UV Index values (black dot) in MCMA for the period 2000-2019: median (central bold line), interquartile range (box edges), 10% and 90% percentiles (the whiskers), the minimum and maximum values (asterisk) and the cosine of the solar zenith angle at solar noon (blue curve).

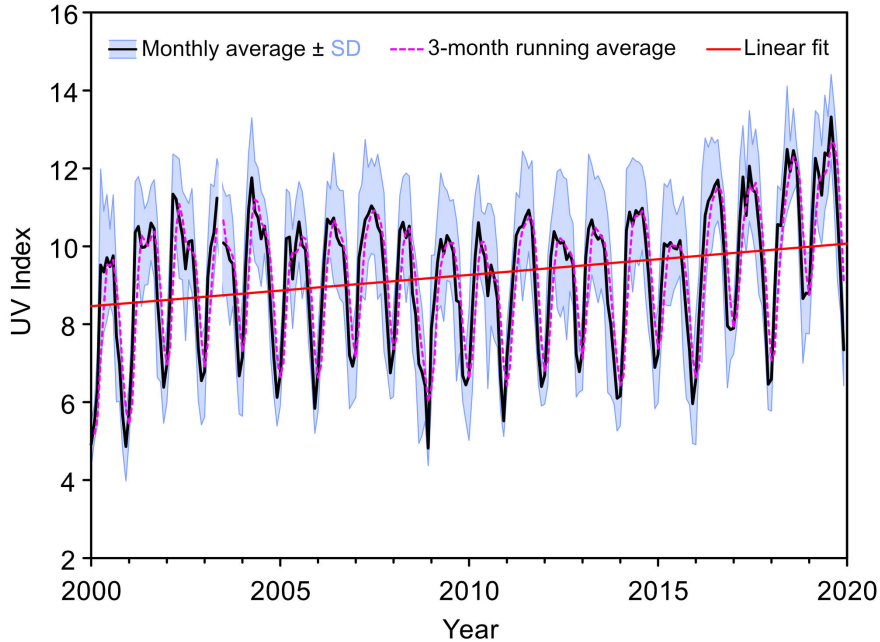


Figure 5: 3-month running average (violet segments curve) applied to monthly average UV Index (black line), the standard deviation (blue fill area) and linear fit (red line).

201        The UV Index computed from satellite-based observations over the period 2005-2019 is  
 202        shown in Figure 6. The satellite-derived UVIs vary from 8 in winter to 16 in summer, both  
 203        values being substantially higher than the ground-based observations (ca. 7 for winter and  
 204        11 for summer, see Fig. 4). We hypothesize that this large difference between satellite-based  
 205        estimation and ground-based observation of the UV index is due to the intense air pollution  
 206        of Mexico City. A rather similar behavior was detected in Santiago city, Chile.<sup>50</sup>

207        Close inspection of Figure 6 shows that the maximum values are reached in June and July  
 208        of each year. While early OMI estimates of the UVI did not account for the boundary layer  
 209        aerosol absorption, the current version (1.3) includes the postcorrection by Arola et al.<sup>51</sup> for  
 210        absorbing aerosols based on global monthly aerosol climatology.

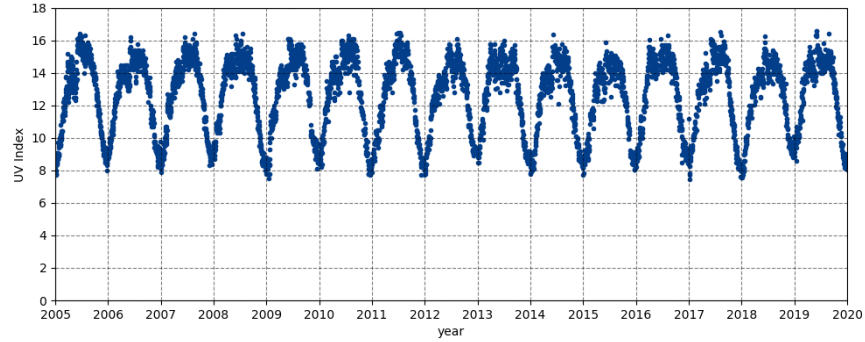


Figure 6: UV Index at solar noon for clear sky recorded by OMI-Aura/NIVR-FMI-NASA, from 2005 to 2019.

## <sup>211</sup> Effect of pollutants on UV radiation

<sup>212</sup> Trends and averages in aerosol optical depth  $AOD_{340}$  and criteria pollutants  $PM_{10}$ , CO,  
<sup>213</sup>  $NO_2$ ,  $O_3$  and  $SO_2$  observed at the SIMAT stations over 2000-2019, are shown in Figure 7  
<sup>214</sup> and summarized in Table 2 together with the  $UVI_{max}$ . Similar trends in pollutants have  
<sup>215</sup> been noted before<sup>52-54</sup> and reflect the long-term success of emission reduction policies and  
<sup>216</sup> programs.

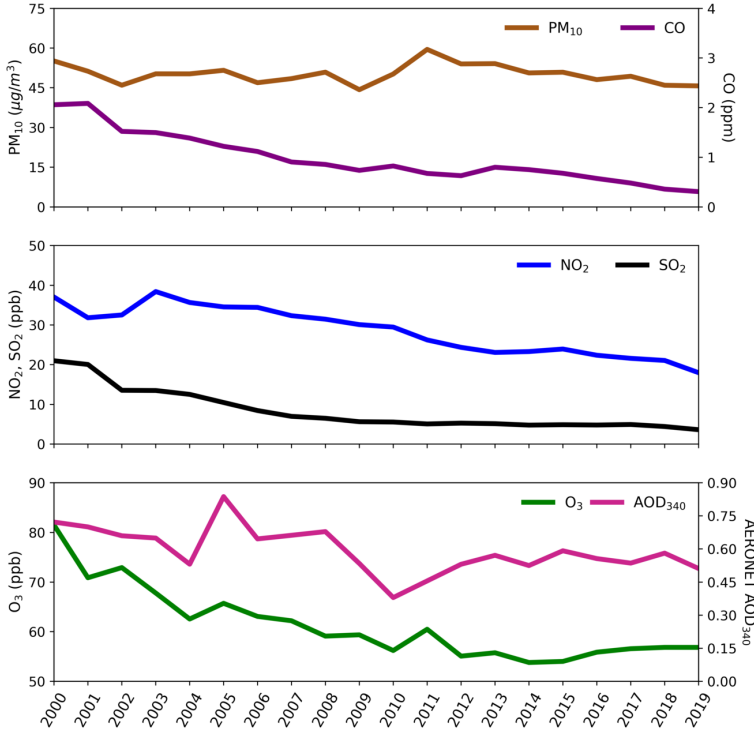


Figure 7: Air quality trends in MCMA for the period 2000-2019 from annual averages obtained between 11h to 15h CST every day: PM<sub>10</sub> (brown curve), CO (purple curve), NO<sub>2</sub> (blue curve), SO<sub>2</sub>(black curve), O<sub>3</sub> (green curve) and AOD<sub>340</sub> (pink curve).

Table 2: UV Index and criteria pollutants: the absolute change per year for the period 2000-2019, averages in units of  $\mu\text{g}/\text{m}^3$ (PM<sub>10</sub>), ppm (CO), ppb (SO<sub>2</sub>, NO<sub>2</sub> and O<sub>3</sub>), dimensionless (UV Index and AOD<sub>340</sub>) and annual percentage change (%/year).

Variable	$\frac{\text{absolutechange}}{\text{year}}$	Avg <sub>2000–2019</sub>	$\Delta(\%/\text{year})$
UVI	0.08	9.2	0.9
PM <sub>10</sub>	-0.10	50.2	-0.2
CO	-0.08	1.0	-8.2
NO <sub>2</sub>	-0.96	28.6	-3.4
O <sub>3</sub>	-1.05	61.3	-1.7
AOD <sub>340</sub>	-0.01	0.6	-1.6
SO <sub>2</sub>	-0.76	8.4	-9.1

The observed changes in the concentrations of these air pollutants have significant implications for surface UV radiation, as can be demonstrated with the TUV radiative transfer model. Table 3 summarizes UVI values for the June-July time period, estimated by the three

220 methods: OMI satellite-derived UVI, SIMAT ground-based observations, and TUV model-  
 221 ing using air pollution estimates. Two groups of values can be readily identified: (1) SIMAT  
 222 daily record values, OMI with or without BL aerosols, and TUV for very clean conditions, all  
 223 with UVI values around 15-16; and (2) the average of daily maxima of SIMAT observations  
 224 and TUV UVI results using MCMA pollutants as input. Note that SIMAT and TUV values  
 225 are in good agreement for both 2018-2019 and 2000-2001 and are considerably lower than for  
 226 case (1). Compared to the OMI estimate that included the climatological aerosol correction  
 227 (15.3), observed SIMAT values were lower by 35% in 2000 and by 20% in 2019. Similarly,  
 228 TUV values were 35% lower in 2000 and 22% lower in 2019 relative to the TUV values of  
 229 15.6 for a pristine atmosphere.

Table 3: UVI maxima for June-July: averages and standard deviation from ground-based data for the years 2018-2019 and 2000-2001. UVI maximum value reached in the period 2000-2019 for UVI ground-based and the same for satellite in the period 2005-2019. TUV calculations for different conditions.

Conditions for estimation in June-July	UV Index
SIMAT average maxima 2000-2001	$9.9 \pm 1.2$
SIMAT average maxima 2018-2019	$12.3 \pm 1.3$
SIMAT maximum value reached in period 2000-2019	15.0
OMI maximum value reached in period 2005-2019, not corrected for BL aerosols	16.6
TUV "zero" pollution	16.1
AOD 0, O <sub>3</sub> 0 ppb, NO <sub>2</sub> 0 ppb, SO <sub>2</sub> 0 ppb	
TUV pristine pollution	15.6
AOD 0.05, O <sub>3</sub> 10 ppb, NO <sub>2</sub> 0 ppb, SO <sub>2</sub> 0 ppb	
TUV 2019:	12.1
AOD 0.5, O <sub>3</sub> 50 ppb, NO <sub>2</sub> 20 ppb, SO <sub>2</sub> 1 ppb	
TUV 2000:	10.2
AOD 0.7, O <sub>3</sub> 70 ppb, NO <sub>2</sub> 40 ppb, SO <sub>2</sub> 20 ppb	

230 The agreement between SIMAT observations and TUV model estimates is excellent but  
 231 also probably a bit fortuitous. Clouds on average reduce the irradiance impinging on the  
 232 surface, but scattering from them can also cause transient enhancements (these are only  
 233 possible if the disk of the Sun is visible) that could be recorded as daily maxima – with  
 234 cancellation between these cloud effects resulting in improved agreement with the cloud-free

model. We cannot exclude that some of the observed trend in UVI is due to changes in cloud cover. However, the modeled fractional UVI reductions due to pollutants, shown in Table 3, are in such good agreement with the observed UVI reductions, that a compelling case can be made for a dominant role of air pollutants in the long-term UVI trends.

Table 4 shows the contributions to UVI reductions from individual pollutants. Aerosols are seen to be the major factor in both time periods, followed by O<sub>3</sub>, NO<sub>2</sub>, and SO<sub>2</sub>. The 2000-2019 UVI increase results in comparable proportions from less aerosols, less SO<sub>2</sub>, and the combined reductions in O<sub>3</sub> and NO<sub>2</sub>.

Comparable UV reductions, of 30-40% due to aerosols, were reported by Panicker et al.<sup>11</sup> over Pune, India from April 2004 to March 2005, with sensitivity coefficients (i.e. change in UVI per unit change in AOD) similar to those found here in Table 3.

Comparisons of OMI with ground-based UV measurements have been reviewed recently by Zhang et al.<sup>55</sup> and Vitt et al.<sup>56</sup>. OMI-derived UV generally overestimates ground-level measurements by 1-10% in relatively clean conditions (e.g. rural U.S), by 10-30% in Southern Europe and by 40% or more in Santiago, Chile<sup>50</sup> and Thailand<sup>57</sup>. The overestimations appear related in large part to incomplete accounting of UV absorption by BL aerosol, although other factors such as the correction to solar noon may also introduce some bias.<sup>55</sup> Over Europe, ground-based UVI observations for several decades are systematically lower than those estimated from satellites even after consideration of climatological aerosol distributions, showing the importance of local pollution not resolved from space.<sup>56</sup> However, difference between satellite-derived and ground-based UVI was less than 1.0 UVI units in over 90% of the cases, in contrast to the difference of 3-5 units found for Mexico City (Table 3).

UV reductions by air pollutants are expected to be most severe near the surface, while chemical reactions leading to photochemical smog occur throughout the vertical extent of the BL. Figure 8 shows the vertical profiles of photolysis coefficients (the reciprocals of photolytic lifetimes) for two key reactions, the photolysis of O<sub>3</sub> to yield excited oxygen atoms O(1D), and the photolysis of NO<sub>2</sub>. In the absence of optically active pollutants, these coefficients

would be nearly independent of altitude in the BL. However, the presence of pollutants leads to a strong decrease toward the surface, with notably more severe reductions in 2000 compared to 2019. While the specific values shown in the figure are only illustrative for typical conditions, routine daily air quality modeling should carefully account for the long term variations in these photolysis coefficients.

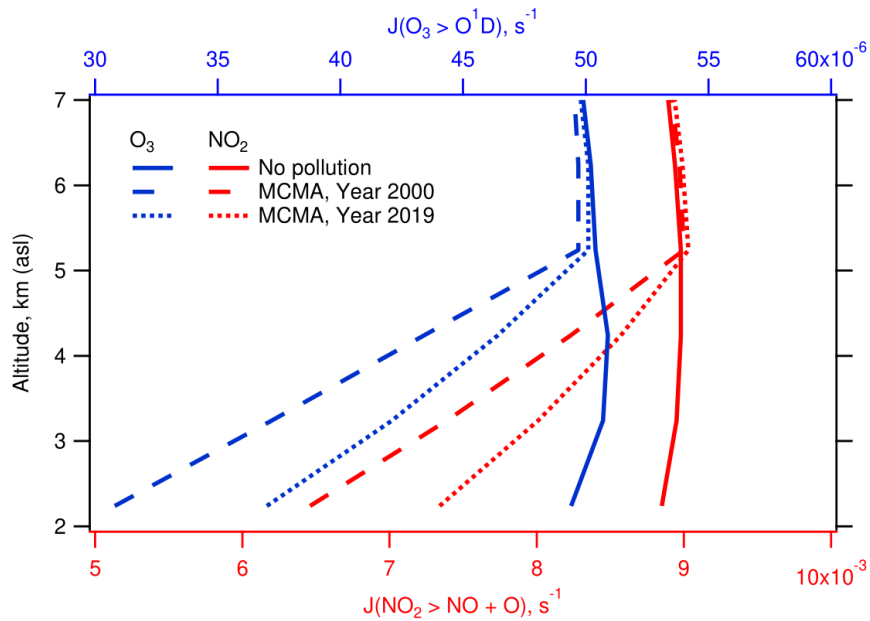


Figure 8: Vertical profiles of the photolysis coefficients for the reaction  $O_3+h\nu \rightarrow O(1D)+O_2$  (top axis, blue)  $NO_2+h\nu \rightarrow O+NO$  (bottom axis, red) for zero pollution (solid) and Mexico City in the years 2000 (dashed) and 2019 (dotted)

An issue that is beginning to gain relevance in radiative balance models is the influence of a group of organic compounds known as “brown carbon” that are capable of strongly absorbing in the UV region.<sup>58</sup> Some of these compounds are related to emissions from local and regional wildfires.<sup>59</sup> Mexico City is frequently exposed to regional fire smoke transport during the dry part of the year (November to May)<sup>60</sup>, which sporadically modify the optical properties of the aerosols.<sup>61</sup> This could partly explain the relatively minor reductions in PM<sub>10</sub> (see Fig. 7), compared to the larger reductions of CO, NO<sub>2</sub>, and O<sub>3</sub> that are more directly related to urban activities, as well as some of the seasonal asymmetry seen in Fig. 3.

276        The UVI is specific to wavelengths mainly in the 300-320 nm range, and so the question  
 277      remains whether these results can be applied at longer UV wavelengths, e.g. those important  
 278      for NO<sub>2</sub> photolysis (<420 nm). Absorption by SO<sub>2</sub> and O<sub>3</sub> vanishes for wavelengths larger  
 279      than about 330 nm, while NO<sub>2</sub> photolysis is mostly driven by UV-A radiation and typical  
 280      aerosols optical depth decrease with wavelength. These changes can easily be modeled, but  
 281      unfortunately far fewer measurements of these longer wavelengths are available in Mexico  
 282      City or elsewhere.

283        Two decades of observations in Mexico City demonstrate unequivocally that air pollution  
 284      reduces UV radiation at the ground. The ground-based observations are well below data  
 285      derived from satellite-based observations. Although ideally both data sets should match,  
 286      the satellite has a limitation to seeing boundary layer absorbers. When typical values of  
 287      the pollutants: aerosols, tropospheric ozone, and to a lesser extent NO<sub>2</sub> and SO<sub>2</sub>, are in-  
 288      cluded in a model (e.g. TUV), the differences between satellite-derived and ground-based  
 289      measured values are explained and can be attributed quantitatively to individual observed  
 290      pollutants. Long term improvements in air quality over the last two decades, are accompa-  
 291      nied by statistically significant increases in the observed UVI, again in good agreement with  
 292      the model-predicted changes.

Table 4: Contributions of individual pollutants to UV Index changes. (a) Values used one at the time, with the others held at zero. (b) UVI deviation from the zero-pollution value of 16.1 (from Table 3). (c) 2019-2000 UVI change due to changes in each pollutant.

Pollutant	Year 2000		Year 2019		2000-2019 (c)
	poll. level (a)	UVI (b)	poll. level	UVI	
AOD	0.7	-3.7	0.5	-2.7	1.0
O <sub>3</sub> ppb (DU)	70 (14)	-1.4	50 (10)	-1.0	0.4
NO <sub>2</sub> ppb	40	-0.9	20	-0.5	0.4
SO <sub>2</sub> ppb	30	-0.8	1	-0.04	0.8

293        The reductions in surface UV radiation with respect to an ideally clear atmosphere –  
 294      by nearly 40% in 2000 and still 20% in 2020 – are large, both within the context of hu-  
 295      man UV exposure and air quality mitigation. In urban areas where ozone production scales

proportionally with UV levels and with volatile organic compound (VOC) emissions (the VOC-limited regime), a 10% increase in BL average photolysis rates means that VOC emissions will need to be reduced by 10% to meet the same goals, or else successful reductions in aerosols would lead to unwanted UV-driven increases in O<sub>3</sub>. Such UV changes must be considered carefully in air quality mitigation strategies. For human exposure, a 20% increase in UV irradiances over two decades should be seen as a non-negligible public health issue requiring some reassessment of preventive behaviors to minimize the risk of skin cancer, cataract, and other UV-related health effects. The efforts that Mexico City has made to improve air quality have reduced levels of most air pollutants. Nevertheless, they caused an increase in UV radiation that reaches the surface.

A limitation of the present work is our focus on daily maximum values, which largely exclude cloud cover. Absorption within clouds can be enhanced by the long path lengths of multiply scattered photons, so that accurate quantification of UV effects of clouds in polluted environments remains a significant challenge and interesting opportunity for future work.

Finally, based on our results, the solar radiation monitoring network could be improved by adding observation sites within or close to the Valley of Mexico, with minor influences of the urban plume (e. g., Amecameca; latitude: 19.13°N, longitude: 99.76°W, elevation: 2420 m asl), and the complementing of sensors in existing monitoring sites that are at elevations above the urban boundary layer like Ajusco (AJU, elevation: 2953 m asl) or Instituto de Investigaciones Nucleares (INN, elevation: 3082 m asl). These sites would provide valuable observations to assess quantitatively the effects of urban pollution on solar radiation levels.

## Acknowledgement

We wish to acknowledge the staff of SIMAT, from the Secretariat of Environment, for the data and the continuous assistance during the realization of this project. Adriana Ipiña would like to extend her thanks to Dirección General de Personal Académico, Universidad Nacional

<sup>321</sup> Autónoma de México (DGAPA-UNAM) for the postdoctoral fellowship at Centro de Ciencias  
<sup>322</sup> de la Atmósfera of the UNAM. Rubén D Piacentini wishes to thank CONICET and National  
<sup>323</sup> University of Rosario, Argentina, for their partial support to the present work. The National  
<sup>324</sup> Center for Atmospheric Research is sponsored by the National Science Foundation.

<sup>325</sup> **References**

- <sup>326</sup> (1) Taylor, H. R.; West, S. K.; Rosenthal, F. S.; Muñoz, B.; Newland, H. S.; Abbey, H.;  
<sup>327</sup> Emmett, E. A. Effect of Ultraviolet Radiation on Cataract Formation. *New England  
Journal of Medicine* **1988**, *319*, 1429–1433.
- <sup>329</sup> (2) Varotsos, C.; Feretis, E. Health effects on human eye resulting from the increased  
<sup>330</sup> ambient solar ultraviolet radiation. *Toxicological & Environmental Chemistry* **1997**,  
<sup>331</sup> *61*, 43–68.
- <sup>332</sup> (3) Lucas, R. M.; Yazar, S.; Young, A. R.; Norval, M.; de Gruijl, F. R.; Takizawa, Y.;  
<sup>333</sup> Rhodes, L. E.; Sinclair, C. A.; Neale, R. E. Human health in relation to exposure to solar  
<sup>334</sup> ultraviolet radiation under changing stratospheric ozone and climate. *Photochemical &  
335 Photobiological Sciences* **2019**, *18*, 641–680.
- <sup>336</sup> (4) Leighton, P. A. *Photochemistry of Air Pollution*; Elsevier, 1961; pp v–vi.
- <sup>337</sup> (5) Seinfeld, J. H.; Pandis, S. N.; Noone, K. Atmospheric Chemistry and Physics: From  
<sup>338</sup> Air Pollution to Climate Change. *Physics Today* **1998**, *51*, 88–90.
- <sup>339</sup> (6) Finlayson-Pitts, B. J.; Pitts, J. N. *Chemistry of the Upper and Lower Atmosphere*;  
<sup>340</sup> Academic Press, 2000; pp xvii–xviii.
- <sup>341</sup> (7) Liu, S. C.; McKeen, S. A.; Madronich, S. Effect of anthropogenic aerosols on biologically  
<sup>342</sup> active ultraviolet radiation. *Geophysical Research Letters* **1991**, *18*, 2265–2268.

- 343 (8) Sabziparvar, A. A.; Forster, P. M. F.; Shine, K. P. Changes in ultraviolet radiation due  
344 to stratospheric and tropospheric ozone changes since preindustrial times. *Journal of*  
345 *Geophysical Research: Atmospheres* **1998**, *103*, 26107–26113.
- 346 (9) Madronich, S.; Wagner, M.; Groth, P. Influence of Tropospheric Ozone Control on  
347 Exposure to Ultraviolet Radiation at the Surface. *Environmental Science & Technology*  
348 **2011**, *45*, 6919–6923.
- 349 (10) McKenzie, R. L.; Weinreis, C.; Johnston, P. V.; Liley, B.; Shiona, H.; Kotkamp, M.;  
350 Smale, D.; Takegawa, N.; Kondo, Y. Effects of urban pollution on UV spectral irradi-  
351 ances. *Atmospheric Chemistry and Physics* **2008**, *8*, 5683–5697.
- 352 (11) Panicker, A. S.; Pandithurai, G.; Takamura, T.; Pinker, R. T. Aerosol effects in the  
353 UV-B spectral region over Pune an urban site in India. *Geophysical Research Letters*  
354 **2009**, *36*, L10802 1–5.
- 355 (12) Palancar, G. G.; Lefer, B. L.; Hall, S. R.; Shaw, W. J.; Corr, C. A.; Herndon, S. C.;  
356 Slusser, J. R.; Madronich, S. Effect of aerosols and NO<sub>2</sub> concentration on ultraviolet  
357 actinic flux near Mexico City during MILAGRO: measurements and model calculations.  
358 *Atmospheric Chemistry and Physics* **2013**, *13*, 1011–1022.
- 359 (13) Bais, A. F.; McKenzie, R. L.; Bernhard, G.; Aucamp, P. J.; Ilyas, M.; Madronich, S.;  
360 Tourpali, K. Ozone depletion and climate change: impacts on UV radiation. *Photo-  
361 chemical & Photobiological Sciences* **2015**, *14*, 19–52.
- 362 (14) Hollaway, M.; Wild, O.; Yang, T.; Sun, Y.; Xu, W.; Xie, C.; Whalley, L.; Slater, E.;  
363 Heard, D.; Liu, D. Photochemical impacts of haze pollution in an urban environment.  
364 *Atmospheric Chemistry and Physics* **2019**, *19*, 9699–9714.
- 365 (15) Li, K.; Jacob, D. J.; Liao, H.; Shen, L.; Zhang, Q.; Bates, K. H. Anthropogenic drivers  
366 of 2013–2017 trends in summer surface ozone in China. *Proceedings of the National  
367 Academy of Sciences* **2018**, *116*, 422–427.

- 368 (16) Wang, Y. et al. *Contrasting trends of PM<sub>2.5</sub> and surface-ozone concentrations in China*  
369 from 2013 to 2017; Oxford University Press (OUP), 2020; Vol. 7; pp 1331–1339.
- 370 (17) Wang, W.; Li, X.; Shao, M.; Hu, M.; Zeng, L.; Wu, Y.; Tan, T. The impact of aerosols  
371 on photolysis frequencies and ozone production in Beijing during the 4-year period  
372 2012–2015. *Atmospheric Chemistry and Physics* **2019**, *19*, 9413–9429.
- 373 (18) Gao, J.; Li, Y.; Zhu, B.; Hu, B.; Wang, L.; Bao, F. What have we missed when studying  
374 the impact of aerosols on surface ozone via changing photolysis rates? *Atmospheric*  
375 *Chemistry and Physics* **2020**, *20*, 10831–10844.
- 376 (19) Bauwens, M.; Compernolle, S.; Stavrakou, T.; Müller, J.-F.; Gent, J.; Eskes, H.; Lev-  
377 elt, P. F.; A, R.; Veefkind, J. P.; Vlietinck, J.; Yu, H.; Zehner, C. Impact of coronavirus  
378 outbreak on NO<sub>2</sub> pollution assessed using TROPOMI and OMI observations. **2020**,  
379 *47*, e2020GL087978.
- 380 (20) Venter, Z. S.; Aunan, K.; Chowdhury, S.; Lelieveld, J. COVID-19 lockdowns cause  
381 global air pollution declines. *Proceedings of the National Academy of Sciences* **2020**,  
382 *117*, 18984–18990.
- 383 (21) Shi, X.; Brasseur, G. P. The Response in Air Quality to the Reduction of Chinese  
384 Economic Activities During the COVID-19 Outbreak. *Geophysical Research Letters*  
385 **2020**, *47*, e2020GL088070.
- 386 (22) Le, T.; Wang, Y.; Liu, L.; Yang, J.; Yung, Y. L.; Li, G.; Seinfeld, J. H. Unexpected air  
387 pollution with marked emission reductions during the COVID-19 outbreak in China.  
388 *Science* **2020**, *369*, 702–706.
- 389 (23) Red Automática de Monitoreo Atmosférico (RAMA). <http://www.aire.cdmx.gob.mx/descargas/datos/excel/RAMAxls.pdf>.

- 391 (24) Doran, J. C. et al. The IMADA-AVER Boundary Layer Experiment in the Mexico City  
392 Area. *Bulletin of the American Meteorological Society* **1998**, *79*, 2497–2508.
- 393 (25) Molina, L. T.; Kolb, C. E.; de Foy, B.; Lamb, B. K.; Brune, W. H.; Jimenez, J. L.;  
394 Ramos-Villegas, R.; Sarmiento, J.; Paramo-Figueroa, V. H.; Cardenas, B.; Gutierrez-  
395 Avedoy, V.; Molina, M. J. Air quality in North America's most populous city – overview  
396 of the MCMA-2003 campaign. *Atmospheric Chemistry and Physics* **2007**, *7*, 2447–2473.
- 397 (26) Molina, L. T. et al. An overview of the MILAGRO 2006 Campaign: Mexico City  
398 emissions and their transport and transformation. *Atmospheric Chemistry and Physics*  
399 **2010**, *10*, 8697–8760.
- 400 (27) Jazcilevich, A. D.; García, A. R.; Caetano, E. Locally induced surface air confluence  
401 by complex terrain and its effects on air pollution in the valley of Mexico. *Atmospheric  
402 Environment* **2005**, *39*, 5481–5489.
- 403 (28) Tie, X.; Madronich, S.; Li, G.; Ying, Z.; Zhang, R.; Garcia, A. R.; Lee-Taylor, J.; Liu, Y.  
404 Characterizations of chemical oxidants in Mexico City: A regional chemical dynamical  
405 model (WRF-Chem) study. *Atmospheric Environment* **2007**, *41*, 1989–2008.
- 406 (29) Zhang, Y.; Dubey, M. K.; Olsen, S. C.; Zheng, J.; Zhang, R. Comparisons of  
407 WRF/Chem simulations in Mexico City with ground-based RAMA measurements dur-  
408 ing the 2006-MILAGRO. *Atmospheric Chemistry and Physics* **2009**, *9*, 3777–3798.
- 409 (30) Zavala, M.; Brune, W. H.; Velasco, E.; Retama, A.; Cruz-Alavez, L. A.; Molina, L. T.  
410 Changes in ozone production and VOC reactivity in the atmosphere of the Mexico City  
411 Metropolitan Area. *Atmospheric Environment* **2020**, *238*, 117747.
- 412 (31) WHO,; WMO,; UNEP,; ICNIRP, *Global solar UV index : a practical guide*; 2002; pp A  
413 joint recommendation of the World Health Organization, World Meteorological Orga-  
414 nization, United Nations Environment Programme, and the International Commission  
415 on Non-Ionizing Radiation Protection.

- 416 (32) Webb, A. R.; Slaper, H.; Koepke, P.; Schmalwieser, A. W. Know Your Standard: Clarifying the CIE Erythema Action Spectrum. *Photochemistry and Photobiology* **2011**, *87*,  
417  
418 483–486.
- 419 (33) Whiteman, C. D.; Zhong, S.; Bian, X.; Fast, J. D.; Doran, J. C. Boundary layer evolution and regional-scale diurnal circulations over the Mexican plateau. *Journal of Geophysical Research: Atmospheres* **2000**, *105*, 10081–10102.  
420  
421
- 422 (34) Fast, J. D.; de Foy, B.; Rosas, F. A.; Caetano, E.; Carmichael, G.; Emmons, L.;  
423 McKenna, D.; Mena, M.; Skamarock, W.; Tie, X.; Coulter, R. L.; Barnard, J. C.;  
424 Wiedinmyer, C.; Madronich, S. A meteorological overview of the MILAGRO field cam-  
425 paigns. *Atmospheric Chemistry and Physics* **2007**, *7*, 2233–2257.
- 426 (35) Carreón-Sierra, S.; Salcido, A.; Castro, T.; Celada-Murillo, A.-T. Cluster Analysis of  
427 the Wind Events and Seasonal Wind Circulation Patterns in the Mexico City Region.  
428 *Atmosphere* **2015**, *6*, 1006–1031.
- 429 (36) Holben, B.; Eck, T.; Slutsker, I.; Tanré, D.; Buis, J.; Setzer, A.; Vermote, E.; Reagan, J.;  
430 Kaufman, Y.; Nakajima, T.; Lavenu, F.; Jankowiak, I.; Smirnov, A. AERONET—A  
431 Federated Instrument Network and Data Archive for Aerosol Characterization. *Remote  
432 Sensing of Environment* **1998**, *66*, 1–16.
- 433 (37) Carabali, G.; Estévez, H. R.; Valdés-Barrón, M.; Bonifaz-Alfonzo, R.; Riveros-  
434 Rosas, D.; Velasco-Herrera, V. M.; Vázquez-Gálvez, F. A. Aerosol climatology over  
435 the Mexico City basin: Characterization of optical properties. *Atmospheric Research*  
436 **2017**, *194*, 190–201.
- 437 (38) NASA EOS/Aura Validation Data Center (AVDC) - Correlative data, Field of  
438 View Predictions, Data Subsets, GEOMS, DCIO. [https://avdc.gsfc.nasa.gov/pub/  
439 most\\_popular/overpass/OMI/](https://avdc.gsfc.nasa.gov/pub/most_popular/overpass/OMI/).

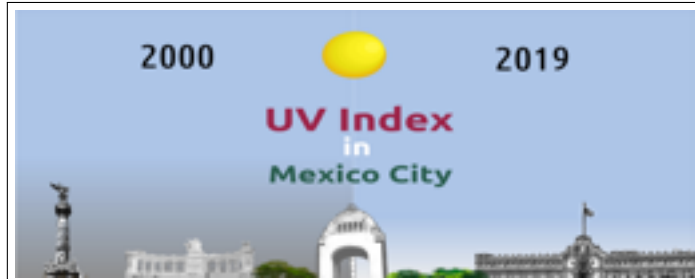
- 440 (39) Tanskanen, A.; Krotkov, N.; Herman, J.; Arola, A. Surface ultraviolet irradiance from  
441 OMI. *IEEE Transactions on Geoscience and Remote Sensing* **2006**, *44*, 1267–1271.
- 442 (40) Madronich, S. Intercomparison of NO<sub>2</sub> photodissociation and U.V. Radiometer Mea-  
443 surements. *Atmospheric Environment* **1987**, *21*, 569–578.
- 444 (41) Shaw, W. J.; Pekour, M. S.; Coulter, R. L.; Martin, T. J.; Walters, J. T. The daytime  
445 mixing layer observed by radiosonde profiler, and lidar during MILAGRO. *Atmospheric*  
446 *Chemistry and Physics Discussions* **2007**, *7*, 15025–15065.
- 447 (42) Velasco, E.; Márquez, C.; Bueno, E.; Bernabé, R. M.; Sánchez, A.; Fentanes, O.; Wöhrn-  
448 schimmel, H.; Cárdenas, B.; Kamilla, A.; Wakamatsu, S.; Molina, L. T. Vertical dis-  
449 tribution of ozone and VOCs in the low boundary layer of Mexico City. *Atmospheric*  
450 *Chemistry and Physics* **2008**, *8*, 3061–3079.
- 451 (43) Greenberg, J.; Guenther, A.; Turnipseed, A. Tethered balloon-based soundings of ozone  
452 aerosols, and solar radiation near Mexico City during MIRAGE-MEX. *Atmospheric*  
453 *Environment* **2009**, *43*, 2672–2677.
- 454 (44) Rogers, R. R.; Hair, J. W.; Hostetler, C. A.; Ferrare, R. A.; Obland, M. D.; Cook, A. L.;  
455 Harper, D. B.; Burton, S. P.; Shinozuka, Y.; McNaughton, C. S.; Clarke, A. D.; Re-  
456 demann, J.; Russell, P. B.; Livingston, J. M.; Kleinman, L. I. NASA LaRC airborne  
457 high spectral resolution lidar aerosol measurements during MILAGRO: observations  
458 and validation. *Atmospheric Chemistry and Physics* **2009**, *9*, 4811–4826.
- 459 (45) Lewandowski, P. A.; Eichinger, W. E.; Holder, H.; Prueger, J.; Wang, J.; Kleinman, L. I.  
460 Vertical distribution of aerosols in the vicinity of Mexico City during MILAGRO-2006  
461 Campaign. *Atmospheric Chemistry and Physics* **2010**, *10*, 1017–1030.
- 462 (46) Corr, C. A.; Krotkov, N.; Madronich, S.; Slusser, J. R.; Holben, B.; Gao, W.; Flynn, J.;  
463 Lefer, B.; Kreidenweis, S. M. Retrieval of aerosol single scattering albedo at ultraviolet

- 464 wavelengths at the T1 site during MILAGRO. *Atmospheric Chemistry and Physics*  
465 **2009**, *9*, 5813–5827.
- 466 (47) Castro, T.; Madronich, S.; Rivale, S.; Muhlia, A.; Mar, B. The influence of aerosols on  
467 photochemical smog in Mexico City. *Atmospheric Environment* **2001**, *35*, 1765–1772.
- 468 (48) SEDEMA, *Calidad del aire en la Ciudad de México, Informe 2017*; 2018.
- 469 (49) Retama, A.; Baumgardner, D.; Raga, G. B.; McMeeking, G. R.; Walker, J. W. Sea-  
470 seasonal and diurnal trends in black carbon properties and co-pollutants in Mexico City.  
471 *Atmospheric Chemistry and Physics* **2015**, *15*, 9693–9709.
- 472 (50) Cabrera, S.; Ipiña, A.; Damiani, A.; Cordero, R. R.; Piacentini, R. D. UV index values  
473 and trends in Santiago Chile ( $33.5^{\circ}\text{S}$ ) based on ground and satellite data. *Journal of*  
474 *Photochemistry and Photobiology B: Biology* **2012**, *115*, 73–84.
- 475 (51) Arola, A. et al. A new approach to correct for absorbing aerosols in OMI UV. *Geophys-  
476 ical Research Letters* **2009**, *36*, L22805 1–5.
- 477 (52) Parrish, D. D.; Singh, H. B.; Molina, L.; Madronich, S. Air quality progress in North  
478 American megacities: A review. *Atmospheric Environment* **2011**, *45*, 7015–7025.
- 479 (53) Secretaría del Medio Ambiente de la Ciudad de México, *Calidad del aire en la Ciudad  
480 de México, informe 2017*; 2018; pp 1–160.
- 481 (54) Molina,; Velasco,; Retama,; Zavala, Experience from Integrated Air Quality Manage-  
482 ment in the Mexico City Metropolitan Area and Singapore. *Atmosphere* **2019**, *10*,  
483 512.
- 484 (55) Zhang, H.; Wang, J.; García, L. C.; Zeng, J.; Dennhardt, C.; Liu, Y.; Krotkov, N. A.  
485 Surface erythemal UV irradiance in the continental United States derived from ground-  
486 based and OMI observations: quality assessment trend analysis and sampling issues.  
487 *Atmospheric Chemistry and Physics* **2019**, *19*, 2165–2181.

- 488 (56) Vitt, R.; Laschewski, G.; Bais, A.; Diémoz, H.; Fountoulakis, I.; Siani, A.-M.;  
489 Matzarakis, A. UV-Index Climatology for Europe Based on Satellite Data. *Atmosphere*  
490 **2020**, *11*, 727.
- 491 (57) Janjai, S.; Wisitsirikun, S.; Buntoung, S.; Pattarapanitchai, S.; Wattan, R.; Masiri, I.;  
492 Bhattarai, B. K. Comparison of UV index from Ozone Monitoring Instrument (OMI)  
493 with multi-channel filter radiometers at four sites in the tropics: effects of aerosols and  
494 clouds. *International Journal of Climatology* **2013**, *34*, 453–461.
- 495 (58) Laskin, A.; Laskin, J.; Nizkorodov, S. A. Chemistry of Atmospheric Brown Carbon.  
496 *Chemical Reviews* **2015**, *115*, 4335–4382.
- 497 (59) Gadhavi, H.; Jayaraman, A. Absorbing aerosols: contribution of biomass burning and  
498 implications for radiative forcing. *Annales Geophysicae* **2010**, *28*, 103–111.
- 499 (60) Rios, B.; Raga, G. B. Smoke emissions from agricultural fires in Mexico and Central  
500 America. *Journal of Applied Remote Sensing* **2019**, *13*, 1.
- 501 (61) Barnard, J. C.; Volkamer, R.; Kassianov, E. I. Estimation of the mass absorption cross  
502 section of the organic carbon component of aerosols in the Mexico City Metropolitan  
503 Area. *Atmospheric Chemistry and Physics* **2008**, *8*, 6665–6679.

504 Graphical TOC Entry

505



Some journals require a graphical entry for the Table of Contents. This should be laid out “print ready” so that the sizing of the text is correct.

Inside the `tocentry` environment, the font used is Helvetica 8 pt, as required by *Journal of the American Chemical Society*.

The surrounding frame is 9 cm by 3.5 cm, which is the maximum permitted for *Journal of the American Chemical Society* graphical table of content entries. The box will not resize if the content is too big: instead it will overflow the edge of the box.

This box and the associated title will always be printed on a separate page at the end of the document.